

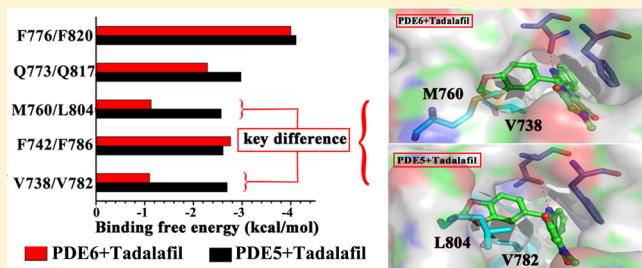
The Molecular Basis for the Selectivity of Tadalafil toward Phosphodiesterase 5 and 6: A Modeling Study

Yi-You Huang, Zhe Li, Ying-Hong Cai, Ling-Jun Feng, Yinuo Wu, Xingshu Li, and Hai-Bin Luo*

School of Pharmaceutical Sciences, Sun Yat-Sen University, Guangzhou 510006, China

Supporting Information

ABSTRACT: Great attention has been paid to the clinical significance of phosphodiesterase 5 (PDES) inhibitors, such as sildenafil, tadalafil, and vardenafil widely used for erectile dysfunction. However, sildenafil causes side effects on visual functions since it shows similar potencies to inhibit PDE5 and PDE6, whereas tadalafil gives a high selectivity of 1020-fold against PDE6. Till now, their molecular mechanisms of selectivity of PDE5 versus PDE6 have remained unknown in the absence of the crystal structure of PDE6. In order to elucidate its isoform-selective inhibitory mechanism, a 3D model of PDE6 was constructed by homology modeling, and its interaction patterns with tadalafil plus sildenafil were exploited by molecular docking, molecular dynamics (MD) simulations, and binding free energy calculations. The present work reveals that tadalafil exhibits a less negative predicted binding free energy of -35.21 kcal/mol with PDE6 compared with the value of -41.12 kcal/mol for PDES, which suggests that tadalafil prefers PDES rather than PDE6 and confers a high selectivity for PDES versus PDE6. The binding free energy results for tadalafil were consistent with external bioassay studies ($IC_{50} = 5100$ and 5 nM toward PDE6 and PDES, respectively). Two important residues from the Q_2 pockets (Val782 and Leu804 in PDES and their corresponding Val738 and Met760 in PDE6) were further identified to account for the high selectivity of tadalafil for PDES versus PDE6. These findings have shed light on the continuous puzzle of why sildenafil ($IC_{50} = 74$ and 6 nM toward PDE6 and PDES, respectively) causes visual disorders because of its poor selectivity but tadalafil does not. In addition, the homology model of PDE6 can be used to design more potent and selective second-generation PDES inhibitors with less inhibitory potency against PDE6.



1. INTRODUCTION

Cyclic nucleotide phosphodiesterases (PDEs) play critical roles in hydrolyzing the cellular second messengers cAMP and cGMP to 5'-AMP and 5'-GMP, respectively. According to their encoding genes and substrate specificity, PDEs can be categorized into 11 families that are distributed in various cellular compartments and are involved in many physiological processes.^{1–7} Now, PDEs serve as important drug targets for the treatment of various diseases such as erectile dysfunction, asthma, and chronic obstructive pulmonary disease and for improving cognitive abilities such as learning and memory.^{8–12} Among the drugs targeting PDE families, the most successful ones are the PDES inhibitors such as sildenafil, tadalafil, vardenafil, and udenafil (Figure 1), which have been widely used for the treatment of male erectile dysfunction.^{13–15} Although the four PDES inhibitors have been successfully approved as drugs, their preclinical and clinical data have revealed transitory but significant effects on visual disorders characterized by low visual acuity and lack of color discrimination, which are supposed to be mainly a result of the inhibition of another enzyme, PDE6.¹⁶

PDE6 is highly concentrated in the outer segments of rod and cone cells of the retina and serves as a key enzyme in visual signal transduction, which is responsible for rapid hydrolysis of

cGMP in response to light stimulation, resulting in the closure of cGMP-gated channels and hyperpolarization of plasma membranes.^{17–23} The rod PDE6 is a heterotetramer consisting of PDE6A and PDE6B catalytic subunits and two identical inhibitory $\beta\gamma$ subunits, while the cone PDE6 is a tetramer comprising two identical PDE6C catalytic subunits and two identical inhibitory $\beta\gamma$ subunits.^{6,24,25} Each of the catalytic subunits contains a homologous C-terminal catalytic domain and two GAF domains (corresponding to cGMP allosteric binding).^{23,26–28}

Among the 11 PDE families, PDE6 is most closely related to PDES on the basis of structure, biochemistry, pharmacologic properties, and substrate specificity, which may give clues to, for example, the side effects of sildenafil on visual function.^{23,28–31} As for the two enzymes, not only do they share good resemblance of molecular organization in terms of primary amino acid sequences, but they are also similar in biochemical properties, such as a preference for cGMP as the substrate over cAMP and a high affinity for cGMP binding at the regulatory GAF domains. Moreover, several inhibitors give similar potencies to inhibit PDES and PDE6. For example, the IC_{50}

Received: August 2, 2013

Published: November 1, 2013



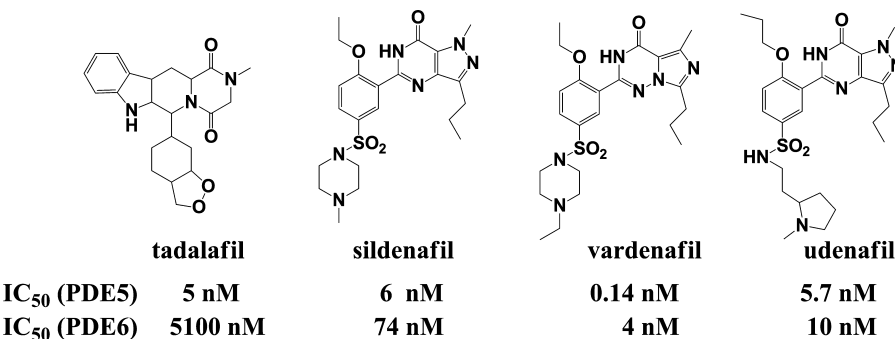


Figure 1. Chemical structures and IC_{50} values³² of important PDES inhibitors approved as drugs.

values of sildenafil toward PDES and PDE6 are 6 and 74 nM, respectively,³² so it is only about 12-fold as potent for PDES as for PDE6. Although the crystal structures of a fully active catalytic domain of unliganded or liganded PDES are available in the Protein Data Bank (PDB) database,^{33–37} the expression of functional PDE6 is extremely difficult to achieve, so as the crystal structure is not attainable yet.^{38–40} Thus, the differences between the catalytic sites in PDES and PDE6 remain unknown.

As the development of the second generation of PDES inhibitors with an enhancement of the selectivity against PDE6 continues,^{36,37,41} the understanding of the molecular architecture of the catalytic site of PDE6, especially the relatively weaker binding with tadalafil, is a necessary requirement. In the present study, a 3D structure of PDE6 was constructed by homology modeling, and ligands (tadalafil, sildenafil, vardenafil, and udenafil) were docked into the modeled structure of PDE6 and the crystal structure of PDES, which were subsequently subjected to relatively long time scale molecular dynamics (MD) simulations and binding free energy calculations. We demonstrate that the relatively high selectivity of tadalafil for PDES versus PDE6 may result from two key residues in the catalytic sites (Val782 and Leu804 in PDES and their corresponding Val738 and Met760 in PDE6) in view of the binding patterns and binding free energies between it and its receptors.

2. COMPUTATIONAL METHODS

2.1. Homology Modeling. On the basis of the theoretical assumption that the structure of a target protein can be predicted by homology modeling from closely related structures,^{42,43} the homology structure of PDE6 was constructed from the crystal counterpart of PDES. Because of a little difference among the sequences of retinal rod and cone PDE6 catalytic subunits,²⁵ only the amino acid sequence of the α subunit of rod PDE6 was extracted from UniProt (www.uniprot.org, access number P16499). Then the template searching was done by the sequence analysis module implemented in Accelrys Discovery Studio 2.5.5.⁴⁴ After BLAST searching over either the NCBI Web site or locally installed databases, several crystal structures of PDES were identified to be candidate templates with respect to high sequence identities and similarities. Then the crystal structure of PDES in complex with sildenafil (PDB code 2H42³⁶) at a resolution of 2.3 Å was selected as the template, and the 3D structure of PDE6 was constructed with the default values of parameters by the MODELER module implemented in Accelrys Discovery Studio 2.5.5.

PDE6 requires two divalent metal ions (Mg^{2+} and Zn^{2+}) bound to the catalytic domain for cGMP hydrolysis,³⁰ so the ions and their coordinated water were also added to the modeled structure on the basis of the alignment with the template structure 2H42 of PDES. The 3D structure of PDE6 was finally evaluated by other protocols implemented in Accelrys Discovery Studio 2.5.5.

After the initial structure of PDE6 was constructed, minimizations to relieve the structure from conflicts, overlaps, and bad contacts with atoms in other residues were carried out by using the sander module of Amber11.⁴⁵ Herein two steps of minimizations were applied, in which a weak constraint of 10 kcal mol⁻¹ Å⁻² on the heavy atoms was used in the first step and no constraint was used in the second step. Each step contained 2500 cycles of the steepest descent method and another 2500 cycles of the conjugate gradient method subsequently. The optimized structure was cautiously checked to make sure that the overall structure did not go through big changes compared with the initial structure.

2.2. Molecular Docking. The interactions between small molecules and receptors were initially explored by docking studies. For PDES and PDE6, hydrogen atoms and charges were added to the systems using the CHARMM force field and the Momany–Rone partial charge method as implemented in Accelrys Discovery Studio 2.5.5.⁴⁴ All ionizable residues in the systems were set to their protonation states at a neutral pH.^{47,48} The zinc and magnesium ions were assigned with a charge of 2+ and the coordinated water around them were also checked. As the fact that the initial structure of PDE6 was well-aligned to the template structure of PDES, sildenafil also fit the catalytic site of the optimized structure of PDE6. Therefore, the active sites of the two proteins were defined by using sildenafil as a reference ligand, and tadalafil was docked into the active sites of the two enzymes using the CDOCKER protocol⁴⁶ embedded in Accelrys Discovery Studio 2.5.5. It is considered that a successful docking holds the root-mean-square deviation (RMSD) value of the optimum pose less than a threshold of 1 Å in reference to the crystal pose.⁴⁷ It is also remarkable that the crystal structure of PDES with bound tadalafil was available (PDB code of 1XOZ),³⁴ but this PDES protein used for crystallization was chimerically hybridized by a replacement with a PDE4D segment (H-loop). The radius of the input site sphere was set as 10 Å from the center of the binding site, and 20 random conformations were generated for each ligand. The rest of docking parameters were set to default values. It is elaborated that there is a common scheme of inhibitor binding to PDEs in which the hydrophobic interactions formed by the conserved hydrophobic residues sandwich ligands in the catalytic site and hydrogen-bonding interactions occur with

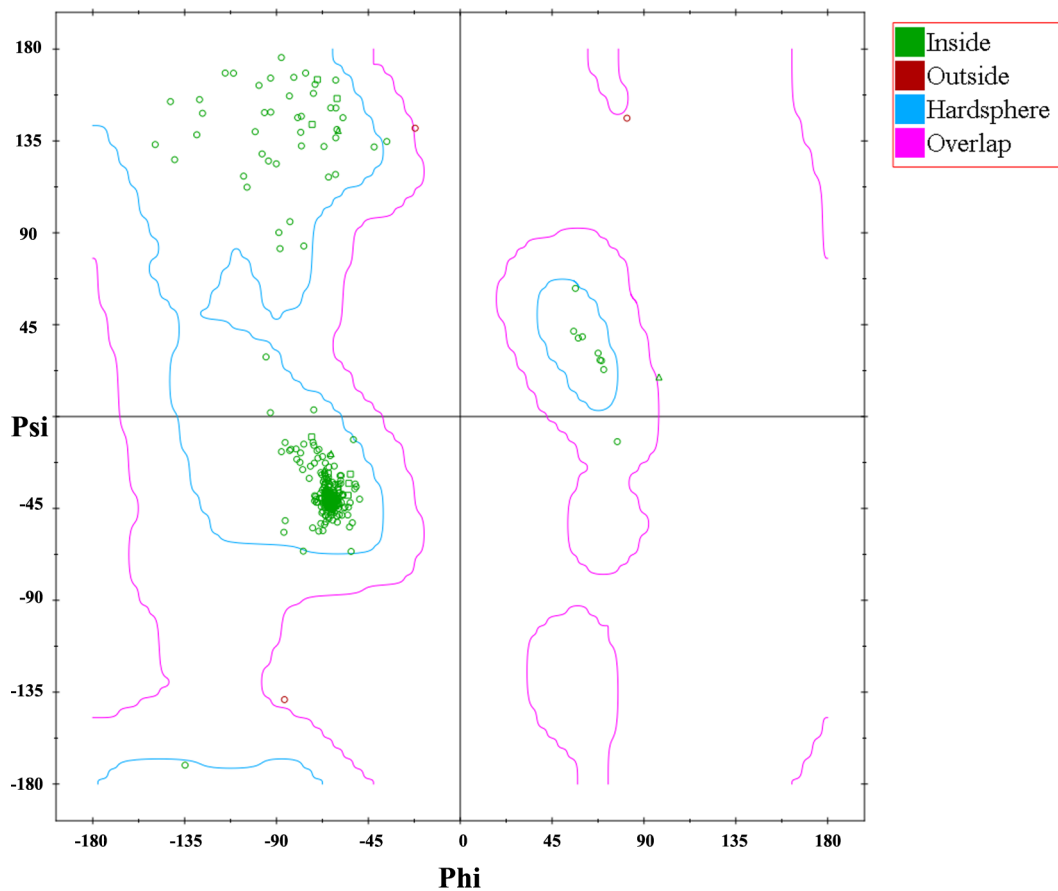


Figure 2. Ramachandran plot of the initial model for PDE6.

the invariant glutamine.³⁴ On the basis of this given scheme, the complex structures of PDES and PDE6 in complex with tadalafil after molecular docking were subjected to MD simulations.

2.3. MD Simulations. In the crystal structure of the catalytic domain of unliganded PDESA1 or PDEA1 occupied by sildenafil or icarisiid II reported by Wang et al.,³⁶ the H-loop (residues 660–683) at the active-site pocket presents four different conformations and migrates as much as 35 Å upon the binding of ligands. Another crystal structure of PDESA1 in complex with vardenafil that was also reported by Wang et al.³⁷ shows that both the protein conformation and the inhibitor configuration are significantly different from the structure in complex with sildenafil. On the basis of these observations and the close relationship between PDES and PDE6, it was reasonable to assume that PDE6 also generates ligand-induced conformation changes upon ligand binding to achieve better fits. Thus, because the protein conformation motions were not considered in the docking procedures,⁴⁷ relatively long time MD simulations ranging from 30 to 150 ns were carried out in order to achieve an equilibrated state for different systems.

On the basis of the molecular docking, nine systems, including the optimized structure of unliganded PDE6 and the complex structures of PDES or PDE6 in complex with sildenafil, tadalafil, vardenafil, or udenafil, were subjected to MD simulations using the sander module of Amber 11.⁴⁵ The parameters for the MD simulations (shown in Appendix 1 in the Supporting Information) were similar to those in our previous studies^{47,48} (e.g., the Zn^{2+} and Mg^{2+} ions were treated by the “nonbond model” method^{49,50} and the water molecule

between them was treated as OH^-), except for the simulation time scale for the production run.

2.4. Binding Free Energy Calculations (ΔG_{bind}). After the MD simulations, the stability of each system was validated in terms of RMSD for the backbone atoms. Then the last period of 30 ns was selected for each system to calculate the binding free energy (ΔG_{bind}) using the molecular mechanics Poisson–Boltzmann surface area (MM-PBSA) method.^{51–58} For each simulated system, the last 30 ns of the trajectory, which was well-equilibrated, was divided into six parts at intervals of 5 ns. Then 200 snapshots were abstracted from each part at regular intervals for ΔG_{bind} calculations.

For each snapshot, the receptor–ligand binding free energy was calculated as the difference between the free energy of the complex ($G_{complex}$) and the sum of the free energies of the protein ($G_{protein}$) and the ligand (G_{ligand}) as shown in the following equation:

$$\Delta G_{bind} = G_{complex} - (G_{protein} + G_{ligand}) \quad (1)$$

ΔG_{bind} can be evaluated as a sum of the molecular mechanics gas-phase binding energy (ΔG_{MM}), the solvation free energy (ΔG_{sol}), and the entropic contribution ($-T\Delta S$) as follows:

$$\Delta G_{bind} = \Delta G_{MM} + \Delta G_{sol} - T\Delta S \quad (2)$$

The MM binding energies consist of the electrostatic and van der Waals interactions (ΔG_{ele} and ΔG_{vdw} respectively) (eq 3), which were calculated by the sander module. The solvation free energy is composed of two components: the polar contribution to solvation ($\Delta G_{ele,sol}$) and the nonpolar solvation term ($\Delta G_{nonpol,sol}$) (eq 4). The former was obtained by solving the

Poisson–Boltzmann equation by means of the MM-PBSA method or generalized Born models by means of MM-GBSA. The latter was determined as a function of the solvent accessible surface area (SASA), which was estimated with the MSMS algorithm at a probe radius of 1.4 Å, using the parameters $\gamma = 0.0072 \text{ kcal mol}^{-1} \text{ Å}^{-2}$ and $\beta = 0$ as developed by Still et al.^{59,60} (eq 5). In general, the normal mode calculation of entropy for large systems is extremely time-consuming and the bindings of similar small molecules to the same receptor usually result in similar entropies, so the entropy contributions $-T\Delta S$ were ignored in the present study to reduce the computational cost.

$$\Delta G_{\text{MM}} = \Delta G_{\text{ele}} + \Delta G_{\text{vdw}} \quad (3)$$

$$\Delta G_{\text{sol}} = \Delta G_{\text{ele,sol}} + \Delta G_{\text{nonpol,sol}} \quad (4)$$

$$\Delta G_{\text{nonpol,sol}} = \gamma \Delta \text{SASA} + \beta \quad (5)$$

Alternatively, binding free energies were calculated via the molecular mechanics generalized Born surface area (MM-GBSA) method in the Prime program⁶¹ embedded in Schrödinger 2012 and the molecular mechanics generalized Born volume integral (MM-GB/VI) method available in MOE 2010.⁶² The Prime MM-GBSA calculations were performed because of its popularity within the industry and its ability to treat the protein structure partly as flexible. Herein, regions within 5 Å from the ligand were treated as flexible where no constraints were kept on these protein atoms, and ΔG_{bind} was calculated from the difference of single-point energies of the unbound receptor, the unbound ligand, and the complex of the representative structures abstracted from the MD trajectories after clustering analysis. For the MOE MM-GB/VI calculations, ΔG_{bind} was obtained from part of the pose rescoring protocol in the docking of sildenafil and tadalafil into PDE5 and PDE6 by using the GB/VI implicit solvent model.⁶³

3. RESULTS AND DISCUSSION

3D Model of PDE6 Built by Homology Modeling. With the given amino acid sequence of the rod PDE6 α subunit, BLAST searching identified several crystal structures as candidate templates. Not surprisingly, most of these structures were related to the crystal counterparts of PDE5 with or without various bound ligands. However, investigations of these structures revealed that several PDE5 proteins used for crystallization are basically inactive or chimerically hybridized by replacement of the PDE5A catalytic domain with a PDE4D segment (H-loop),²⁴ while some others that used fully native PDE5 are disordered in some flexible loops.³⁶ In the present work, the structure of PDE5 with bound sildenafil (PDB code 2H42) was chosen as the template, taking into consideration its integral and wild-type protein. As shown in Appendix 2 in the Supporting Information, the alignment of sequences in the catalytic domains between PDE5 and PDE6 revealed a sequence identity and similarity of 41.4% and 69.3%, respectively. After its construction by MODELER, the 3D structure of PDE6 was evaluated subsequently by visual inspection of its Ramachandran plot (Figure 2) where more than 98% of the residues are located in the favored $\varphi-\psi$ regions. In addition, the probability density function (PDF) was also checked, and it indicated that the modeled structure was reasonable. On the basis of the structural superposition between PDE5 and PDE6, the two metal ions (Mg^{2+} and

Zn^{2+}) and their coordinated water in the catalytic site of PDE6 were added manually according to their locations in PDE5.

As shown in Figure 3, the initial structure of PDE6 mostly resembles PDE5 except for the β -hairpin region, which is

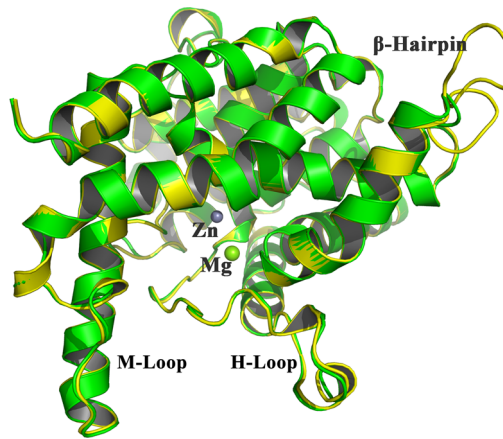


Figure 3. Overall structure of PDE6 after homology modeling (yellow) aligned with the template structure of PDE5 (PDB code 2H42) (green).

relatively short in PDE5 and extended in PDE6. This loop seems to be very important for structural folding of PDE6, since its replacement by PDE5 β -hairpin leads to insoluble and inactive PDE6 expression.⁴⁰ This specific region in PDE6 serves as a linkage for the helices constructing the catalytic active site and is supposed to undergo great fluctuations during the MD simulations to get closer to the wild-type structure. The process of energy minimization eliminated some local conflicts and overlaps among atoms, while the overall structure did not change too much. Thus, a reasonable structure of PDE6 was obtained and used for further analysis.

Validation of Molecular Docking and MD Parameters.

To examine the reliability of the CDOCKER protocol for molecular docking, the crystallized sildenafil in 2H42 was extracted and redocked into the catalytic pocket of PDE5 via various docking conditions and scoring functions. The average RMSD for the top 10 docking poses was 0.8 Å for this case. In addition, another PDE5 inhibitor, vardenafil, which is very similar to sildenafil, was also used to check the applicability of this docking method. In contrast to bound sildenafil, vardenafil bound to PDE5 with the ethylpiperazine portion oriented toward the surface of the catalytic pocket in the docking result, which is very similar to the binding of vardenafil in the crystal structure³⁷ (Figure 4). Both the relatively low redocking RMSD value of sildenafil and the reproducibility of vardenafil's configuration confirmed that the docking method was suitable for this system.

In order to evaluate the MD parameters used, the RMSDs for the backbone atoms were monitored to validate the stabilities of each system along the long-time MD simulations. After a period of disturbance due to the ligand-induced fitting, the RMSD curves of the liganded PDE5 and PDE6 complexes were converged and well-equilibrated after 30 ns (100 ns for the complex between PDE6 and tadalafil) (Figure 5). As shown in Figure 6, the stabilities of the systems were also verified by analysis of the hydrogen bonding between tadalafil and PDE5 or PDE6.

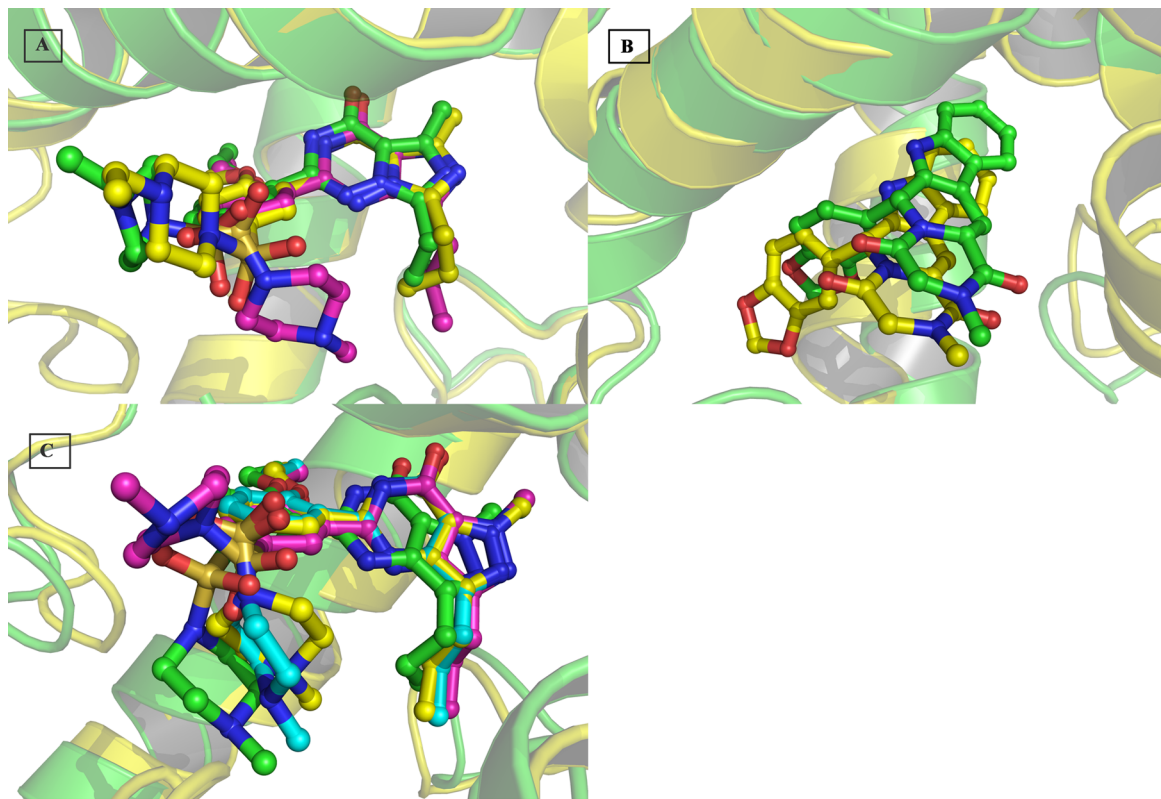


Figure 4. Superpositions of the modeling structures and the crystal counterparts for PDE5. (A) Superposition of crystallized sildenafil (red, PDB code 2H42³⁶), docked vardenafil (yellow), and crystallized vardenafil (green, PDB code 3B2R³⁷) in the catalytic pocket of PDE5. (B) Superposition of tadalafil from the MD-simulated structure (yellow) and the crystal structure (green, PDB code 1XOZ³⁴). (C) Superposition of sildenafil from the MD-simulated structure (blue) and crystal structures by Wang et al.³⁶ (yellow), Zhang et al.³⁵ (green), and Sung et al.³³ (red).

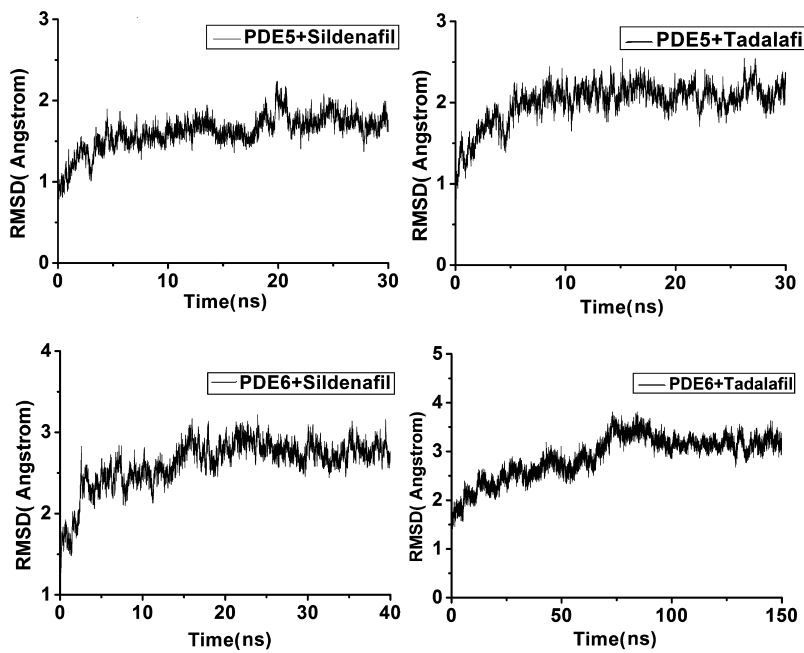


Figure 5. Plots of RMSD for all of the backbone atoms (\AA) vs simulation time (ns) for PDE5 or PDE6 in complex with sildenafil or tadalafil. The RMSD is the root-mean-square deviation of the simulated positions of the backbone atoms (C, N, and C_{α}) of the proteins from those in the initial X-ray crystal structures.

Furthermore, comparisons between the MD-simulated structures and the crystal structures were performed to check the reliability of our MD parameters, as shown in Figure 4. For the crystal structure of PDE5 in complex with sildenafil (Figure

4C), little changes occurred during the MD simulations except for the orientation of the methylpiperazine portion in sildenafil, which was also observed in crystals produced by other groups.^{33,35,37} Besides, the configuration of tadalafil with

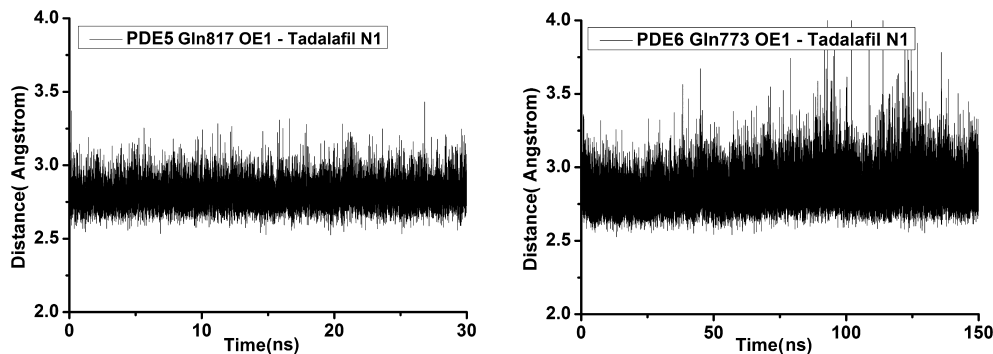


Figure 6. Key distances of hydrogen bonds (\AA) vs simulation time (ns) for (left) PDE5 and (right) PDE6 in complex with tadalafil.

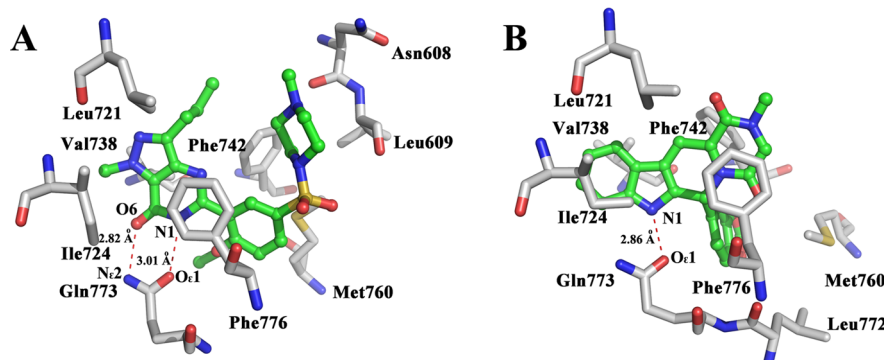


Figure 7. Binding patterns of (A) sildenafil and (B) tadalafil in the catalytic pocket of PDE6 after MD simulations.

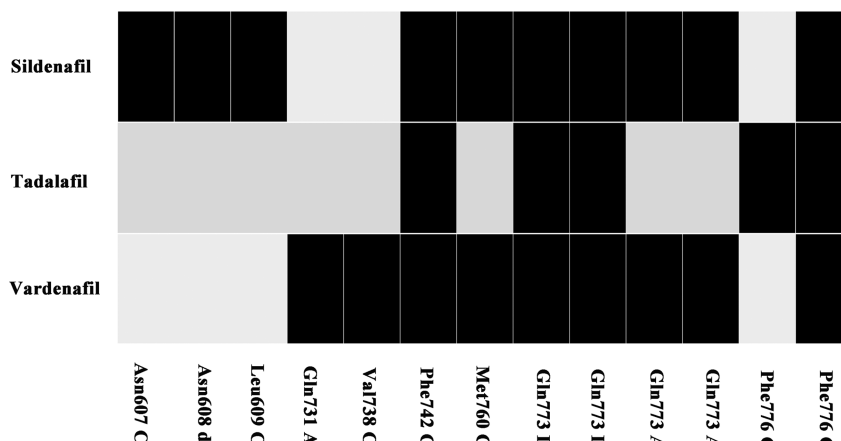


Figure 8. Protein–ligand interaction fingerprints (PLIFs) of PDE6 in complex with sildenafil, tadalafil, and vardenafil generated by MOE 2010. The characters A, D, d, and C represent side-chain hydrogen-bond acceptor, side-chain hydrogen-bond donor, backbone hydrogen-bond donor, and surface contact, respectively. The black areas represent the interactions between PDE6 and the ligands.

PDES was well-aligned with that in the crystal structure (PDB code 1XOZ;³⁴ Figure 4B). Only one hydrogen bond was formed with Phe817, which is also consistent with the crystal structure.³⁴ Therefore, the equilibria and similarities of the PDES systems indicated that the MD parameters we used were appropriate.

Binding Patterns of Sildenafil and Tadalafil with PDE6. The modeled structures of PDE6 in complex with sildenafil and tadalafil after MD simulations are given in Figure 7.

Sildenafil Binds to PDE6 and PDE5 in a Similar Pattern. Sildenafil was partially buried in the catalytic pocket of PDE6 and shared good similarities to its binding with PDES, involving two hydrogen bonds (3.01 and 2.82 \AA , respectively) formed

between N1 and O6 of the imidazotriazinone and O_e1 and N_e2 of Gln773 in PDE6. The distances of the two corresponding hydrogen bonds in structure 2H42 for PDES with bound sildenafil are 3.14 and 2.91 \AA , respectively. For hydrophobic interactions, the large portion of the imidazotriazinone of sildenafil was sandwiched by Phe776, Ile724, Leu721 and Val738, Phe742, Ala735 and also contacted remotely with Leu772 and Tyr558. The methylpiperazine portion is surrounded by Met760, Asn608, Leu609, and Phe742 via van der Waals interactions. The similarities between the binding of sildenafil with PDE6 and that with PDES may account for its similar inhibitory potencies toward the two enzymes.

Tadalafil Binds to PDE6 Very Distinctively from Sildenafil. Because of its special chemical properties, tadalafil was expected

Table 1. Comparison of Binding Free Energies (ΔG_{bind} , kcal/mol) Obtained by Different Methods and Correlations with Their in Vitro Inhibitory Activities (IC_{50})³²

	sildenafil		tadalafil		vardenafil		udenafil	
	PDE5	PDE6	PDE5	PDE6	PDE5	PDE6	PDE5	PDE6
Amber MM-PBSA	-42.63	-40.47	-41.12	-35.21	-43.80	-42.19	-42.41	-41.19
MOE MM-GB/VI	-33.00	-29.45	-24.26	-23.90	-24.56	-24.66	-24.04	-25.03
Prime MM-GBSA	-45.82	-54.00	-59.40	-56.90	-38.931	-43.71	-65.58	-37.42
IC_{50} (nM)	6	74	5	5100	0.14	4	5.7	10

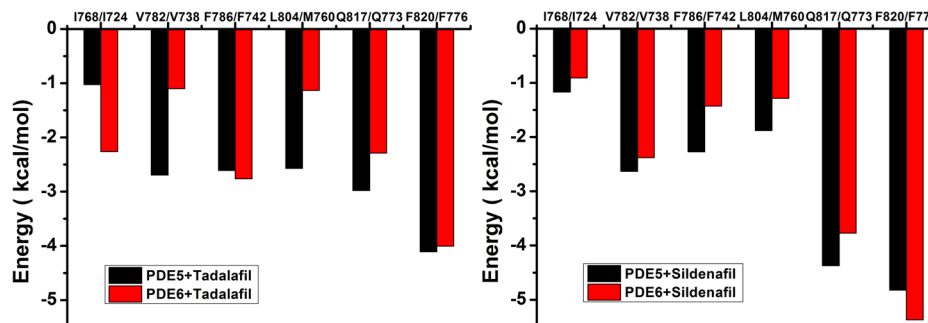


Figure 9. Comparison of the most important residues contributing to the binding free energies (ΔG_{bind}) for (A) tadalafil and (B) sildenafil with PDE5 and PDE6 from energy decomposition.

to bind to PDE6 in a different pattern from sildenafil. Obviously, only one hydrogen bond of 2.86 Å was formed between N1 of the indole ring of tadalafil and O_e1 of Gln773 with an orientation of its γ -amide group by 90° compared with sildenafil. However, the hydrophobic interactions were the predominant forces in the binding of tadalafil. The nearly flat four-ring portion of the pyrazinopyridoindoledione was sandwiched by Phe776, Leu721, Ile724, Val738, Ala739, and Phe742. The methylenedioxyphenyl group of tadalafil was implanted in a hydrophobic pocket consisting of hydrophobic residues such as Phe742, Trp743, Ala739, Met760, Leu769, and Leu772. Despite the lack of one hydrogen bond with the receptor, the hydrophobic interactions make a compensation for its inhibitory potency.

In order to locate the important residues that commonly interact with inhibitors in the catalytic pocket of PDE6, the structures of PDE6 in complex with tadalafil, sildenafil, and vardenafil (achieving its equilibrium under identical conditions after 30 ns MD simulations) from the MD simulated trajectories were analyzed by using the protein–ligand interaction fingerprints (PLIF) module implemented in MOE 2010. As shown in Figure 8, tadalafil mainly interacts with three residues (Phe742, Gln773, and Phe776) in the active-site pocket. However, interactions between PDE6 and sildenafil or vardenafil involve extended hydrogen binding with Asn607, Asn608, and Gln731 as well as extended hydrophobic interactions with Leu609, Val738, and Met760. These extensions might provide a partial explanation for the high inhibition but also weak selectivity of sildenafil or vardenafil (PDE5 versus PDE6), which could be helpful in the design of more selective PDE5 inhibitors.

Unlike the systems for PDE6 with bound ligands, blank PDE6 could not be equilibrated even after 100 ns MD simulations. Similar to PDE5, the H-loop and M-loop of PDE6 were especially flexible and went closer during the MD simulations, which may be due to the formed hydrophobic interactions among residues along the pocket. As a result, the binding pocket of PDE6 was narrowed and collapsed, which

could probably lead to aggregation in biological systems. This assumption may show some implications for the expression failure of PDE6 in various systems; the biggest difference between the PDE5 and PDE6 sequences lies in the extended β -hairpin of PDE6, and how to deal with this section may be a key to the solution of the problem. Furthermore, the ligands stabilized the binding site pocket, so the addition of a special stabilizing agent may be helpful to get the functional and active PDE6.⁶⁴

Binding Free Energies and Drug Selectivity. The binding free energies ΔG_{bind} for the complexes of PDE5 and PDE6 with bound ligands are summarized in Table 1. These values were calculated by using three methods, namely, Amber MM-PBSA, Prime MM-GBSA, and MOE MM-GB/VI. Because of the neglect of the entropic contribution in Amber MM-PBSA, overestimated calculations of ΔG_{bind} with respect to their absolute binding free energies likely occurred. However, the calculated ΔG_{bind} values for these complexes are expected to theoretically/qualitatively reflect their relative in vivo activities.

Analyses of Binding Free Energies Suggest That Tadalafil Prefers PDE5 Rather Than PDE6. On the basis of the Amber MM-PBSA calculations, the ΔG_{bind} values for the binding of sildenafil with PDE5 and PDE6 are -42.63 and -41.12 kcal/mol, respectively, which are consistent with its similar inhibitory affinities (IC_{50} values of 6 and 74 nM,³² respectively; Table 1). Tadalafil exhibits a less negative ΔG_{bind} of -35.21 kcal/mol with PDE6 compared with -41.12 kcal/mol with PDE5. The difference of 5.91 kcal/mol in the binding free energies confers a high selectivity of tadalafil for PDE5 versus PDE6, which suggests that tadalafil prefers PDE5 rather than PDE6. In view of their in vivo inhibitory activities, it displays a great selectivity of 1020-fold toward PDE5 versus PDE6 (IC_{50} of 5 vs 5100 nM, respectively),³² which is consistent with our MM-PBSA ΔG_{bind} results. For the other two small molecules vardenafil and udenafil, it was also found that the MM-PBSA ΔG_{bind} results correlate well with their in vitro inhibitory potencies, as was the case for sildenafil and tadalafil, which

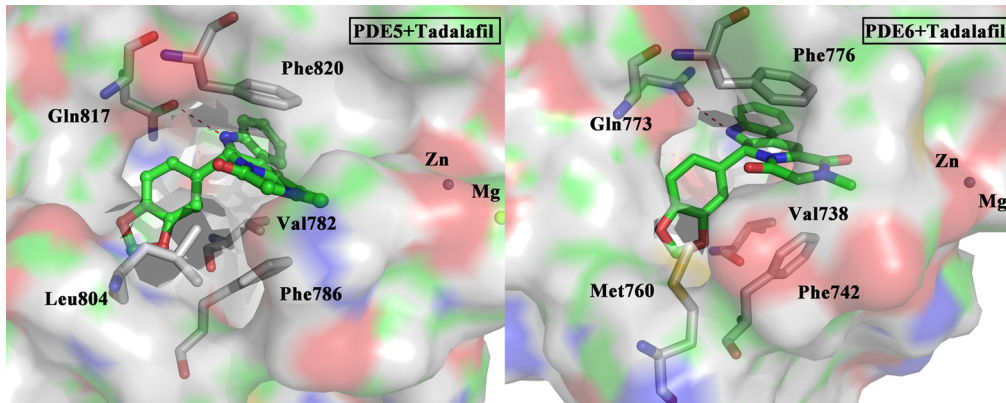


Figure 10. Surface representations of the binding of tadalafil within the active-site pockets of PDE5 and PDE6 showing the replacement of Leu804 in PDE5 with Met760 in PDE6.

suggests that our method for the binding free energy calculation is reliable. In addition, our ΔG_{bind} calculations suggest that the Amber MM-PBSA method is more suitable for the prediction of ΔG_{bind} for the complexes between PDE5/6 and ligands than the Prime MM-GBSA and MOE MM-GB/VI methods.

Two Key Residues May Account for the Relatively High Selectivity of Tadalafil. The selective potency of PDE5 versus PDE6 for tadalafil is of great importance compared with other drugs. To further elaborate the key differences between the binding of tadalafil with PDE5 and that with PDE6, the calculated ΔG_{bind} values were decomposed into single-residue contributions using the MM-GBSA method^{50–58} with the default parameters embedded in Amber 11. Figure 9 lists the most important residues contributing to the binding free energies for the two complexes. In general, if the decomposed energy of a residue is more negative than -1.0 kcal/mol , the residue would be important in the molecular recognition of ligands. Without doubt, hydrogen bonding with the invariant glutamine and $\pi-\pi$ stacking with conserved phenylalanine are the predominant interactions. Furthermore, the results also demonstrate that the encouraging selectivity of tadalafil for PDE5 versus PDE6 mainly results from the different interactions with two key hydrophobic residues. Val782^{PDE5} (-2.89 kcal/mol) and Leu804^{PDE5} (-2.57 kcal/mol) interact with tadalafil more strongly than the corresponding Val738^{PDE6} (-1.10 kcal/mol) and Met760^{PDE6} (-1.13 kcal/mol) in PDE6, whereas for sildenafil, the binding free energies for Val782^{PDE5} (-2.63 kcal/mol) and Val738^{PDE6} (-2.38 kcal/mol) are similar, as are those for Leu804^{PDE5} (-1.88 kcal/mol) and Met760^{PDE6} (-1.28 kcal/mol). A total difference of 3.23 kcal/mol in the binding free energies for the two residues with tadalafil is produced, which might contribute to its high selectivity ($IC_{50} = 5$ and 5100 nM toward PDE5 and PDE6, respectively).

The locations of these key residues reveal a hydrophobic pocket known as the Q₂ pocket³⁴ (Figure 10), which mainly consists of hydrophobic residues that are less conserved compared with other regions in the catalytic domain among different PDE families. In the complexes of PDE5 and PDE6 bound with tadalafil, the methylenedioxophenyl group occupies this very pocket for its special chemical nature, and replacement of Leu804 in PDE5 with Met760 in PDE6 sharply affects the interactions. In view of the fact that the low-selectivity inhibitors such as sildenafil and vardenafil have almost no contacts with this Q₂ pocket, enhanced interactions with this

region may help to exploit selective inhibitors of PDE5 that avoid visual disorders.

4. CONCLUSION

In the present study, a reasonable 3D structure of PDE6 was built through homology modeling, and its binding patterns with sildenafil and tadalafil were explored using molecular docking and MD simulations. The unliganded PDE6 model was very flexible and hardly equilibrated even after 100 ns MD simulations, whereas the liganded PDE6 systems were stable. Our results suggest that the ligands could stabilize the binding site pocket of PDE6 and that addition of a special stabilizing agent may be helpful to get the functional and active PDE6.

The similar potencies of sildenafil to inhibit PDE5 and PDE6 can be attributed to similar interaction patterns with the catalytic pockets of the two enzymes. In contrast, tadalafil can strongly interact with the Q₂ pocket in PDE5, and replacement of Leu804 in this Q₂ pocket with Met760 in PDE6 may lead to a decrease in the binding affinity between PDE6 and tadalafil, which possibly enhances its selectivity for PDE5 versus PDE6. These findings have thrown light on the continuous puzzle that sildenafil causes visual disorders but tadalafil does not. In addition, the homology model of PDE6 can be used to design novel and selective second-generation PDE5 inhibitors that avoid disorders in visual functions with less potency against PDE6.

The current combinatorial approaches, including homology modeling, molecular docking, MD simulations, and MM-PB/GBSA binding free energy calculations, would be useful for the exploratory study of some biological systems for drug discovery purposes, especially for cases where it is difficult to obtain the crystal structure of a receptor/ligand complex, such as the PDE6/tadalafil complex.

■ ASSOCIATED CONTENT

S Supporting Information

Molecular dynamics simulations (Appendix 1) and sequence alignment of the catalytic domains of human PDE6A and PDE5A (Appendix 2). This material is available free of charge via the Internet at <http://pubs.acs.org>.

■ AUTHOR INFORMATION

Corresponding Author

*Tel.: 86-20-39943031. E-mail: luohb77@mail.sysu.edu.cn or luohb77@hotmail.com.

Notes

The authors declare no competing financial interest.

ACKNOWLEDGMENTS

We cordially thank the High Performance Supercomputer Center at Sun Yat-Sen University. This work was supported by the National Natural Science Foundation of China (21103234 and 81373258), the Guangdong Natural Science Foundation (S2011030003190 and S2013010014867), the Guangdong Science Foundation (2012A080201007), the Guangdong Provincial Key Laboratory of Construction Foundation (2011A060901014), the Science Foundation of the Department of Education in Guangdong Province (CXZD1006), and the Fundamental Research Funds for the Central Universities (11ykzd05).

REFERENCES

- (1) Manganiello, V. C.; Taira, M.; Degerman, E.; Belfrage, P. Type III cGMP-inhibited cyclic nucleotide phosphodiesterases (PDE 3 gene family). *Cell. Signaling* **1995**, *7*, 445–455.
- (2) Soderling, S. H.; Beavo, J. A. Regulation of cAMP and cGMP signaling: New phosphodiesterases and new functions. *Curr. Opin. Cell Biol.* **2000**, *12*, 174–179.
- (3) Mehats, C.; Andersen, C. B.; Filopanti, M.; Jin, S. L. C.; Conti, M. Cyclic nucleotide phosphodiesterases and their role in endocrine cell signaling. *Trends Endocrinol. Metab.* **2002**, *13*, 29–35.
- (4) Goraya, T. A.; Cooper, D. M. F. Ca²⁺-calmodulin-dependent phosphodiesterase (PDE1): Current perspectives. *Cell. Signaling* **2005**, *17*, 789–797.
- (5) Bender, A. T.; Beavo, J. A. Cyclic nucleotide phosphodiesterases: Molecular regulation to clinical use. *Pharmacol. Rev.* **2006**, *58*, 488–520.
- (6) Conti, M.; Beavo, J. Biochemistry and physiology of cyclic nucleotide phosphodiesterases: Essential components in cyclic nucleotide signaling. *Annu. Rev. Biochem.* **2007**, *76*, 481–511.
- (7) Omori, K.; Kotera, J. Overview of PDEs and their regulation. *Circ. Res.* **2007**, *100*, 309–327.
- (8) Castro, A.; Jerez, M. J.; Gil, C.; Martinez, A. Cyclic nucleotide phosphodiesterases and their role in immunomodulatory responses: Advances in the development of specific phosphodiesterase inhibitors. *Med. Res. Rev.* **2005**, *25*, 229–244.
- (9) Houslay, M. D.; Schafer, P.; Zhang, K. Y. J. Keynote review: Phosphodiesterase-4 as a therapeutic target. *Drug Discovery Today* **2005**, *10*, 1503–1519.
- (10) Menniti, F. S.; Faraci, W. S.; Schmidt, C. J. Phosphodiesterases in the CNS: Targets for drug development. *Nat. Rev. Drug Discovery* **2006**, *5*, 660–670.
- (11) Meng, F.; Hou, J.; Shao, Y. X.; Wu, P. Y.; Huang, M.; Zhu, X.; Cai, Y. H.; Li, Z.; Xu, J.; Liu, P. Q.; Luo, H.-B.; Wan, Y.-Q.; Ke, H. Structure-based discovery of highly selective phosphodiesterase-9A inhibitors and implications for inhibitor design. *J. Med. Chem.* **2012**, *55*, 8549–8558.
- (12) Lipworth, B. J. Phosphodiesterase-4 inhibitors for asthma and chronic obstructive pulmonary disease. *Lancet* **2005**, *365*, 167–175.
- (13) Gupta, M.; Kovar, A.; Meibohm, B. The clinical pharmacokinetics of phosphodiesterase-5 inhibitors for erectile dysfunction. *J. Clin. Pharmacol.* **2005**, *45*, 987–1003.
- (14) Briganti, A.; Salonia, A.; Deho, F.; Zanni, G.; Barbieri, L.; Rigatti, P.; Montorsi, F. Clinical update on phosphodiesterase type-5 inhibitors for erectile dysfunction. *World J. Urol.* **2005**, *23*, 374–384.
- (15) Lincoln, T. M. Cyclic GMP and phosphodiesterase 5 inhibitor therapies: What's on the horizon? *Mol. Pharmacol.* **2004**, *66*, 11–13.
- (16) Marmor, M. F.; Kessler, R. Sildenafil (Viagra) and ophthalmology. *Surv. Ophthalmol.* **1999**, *44*, 153–162.
- (17) Ames, A.; Walseth, T. F.; Heyman, R. A.; Barad, M.; Graeff, R. M.; Goldberg, N. D. Light-induced increases in cGMP metabolic flux correspond with electrical responses of photoreceptors. *J. Biol. Chem.* **1986**, *261*, 13034–13042.
- (18) Copenhagen, D. R.; Jahr, C. E. Release of endogenous excitatory amino acids from turtle photoreceptors. *Nature* **1989**, *341*, 536–539.
- (19) Baylor, D. How photons start vision. *Proc. Natl. Acad. Sci. U.S.A.* **1996**, *93*, 560–565.
- (20) Pugh, E. N., Jr.; Lamb, T. D. Phototransduction in vertebrate rods and cones: Molecular mechanisms of amplification, recovery and light adaptation. In *Molecular Mechanisms in Signal Transduction*; Stavenga, D. G., Degrip, W. J., Pugh, E. N., Jr., Eds.; Handbook of Biological Physics, Vol. 3; Elsevier: Amsterdam, 2000; Chapter 5, pp 183–255.
- (21) Witkovsky, P.; Thoreson, W.; Tranchina, D. Transmission at the photoreceptor synapse. In *Concepts and Challenges in Retinal Biology*; Kolb, H., Ripps, H., Wu, S., Eds.; Progress in Brain Research, Vol. 131; Elsevier: Amsterdam, 2001; Chapter 9, pp 145–159.
- (22) Arshavsky, V. Y.; Lamb, T. D.; Pugh, E. N., Jr. G proteins and phototransduction. *Annu. Rev. Physiol.* **2002**, *64*, 153–187.
- (23) Cote, R. H. Characteristics of Photoreceptor PDE (PDE6): Similarities and differences to PDE5. *Int. J. Impot. Res.* **2004**, *16*, S28–S33.
- (24) Hamilton, S. E.; Hurley, J. B. A phosphodiesterase inhibitor specific to a subset of bovine retinal cones. *J. Biol. Chem.* **1990**, *265*, 11259–11264.
- (25) Muradov, H.; Boyd, K. K.; Artemyev, N. O. Rod phosphodiesterase-6 PDE6A and PDE6B subunits are enzymatically equivalent. *J. Biol. Chem.* **2010**, *285*, 39828–39834.
- (26) Norton, A. W.; D'Amours, M. R.; Grazio, H. J.; Hebert, T. L.; Cote, R. H. Mechanism of transducin activation of frog rod photoreceptor phosphodiesterase: Allosteric interactions between the inhibitory γ subunit and the noncatalytic cGMP-binding sites. *J. Biol. Chem.* **2000**, *275*, 38611–38619.
- (27) Mou, H.; Cote, R. H. The catalytic and GAF domains of the rod cGMP phosphodiesterase (PDE6) heterodimer are regulated by distinct regions of its inhibitory γ subunit. *J. Biol. Chem.* **2001**, *276*, 27527–27534.
- (28) Tchoudji, J. F. K.; Lebeau, L.; Virmaux, N.; Maftei, C. G.; Cote, R. H.; Lugnier, C.; Schultz, P. Molecular organization of bovine rod cGMP-phosphodiesterase 6. *J. Mol. Biol.* **2001**, *310*, 781–791.
- (29) McAllister-Lucas, L. M.; Sonnenburg, W. K.; Kadlecak, A.; Seger, D.; Trong, H. L.; Colbran, J. L.; Thomas, M. K.; Walsh, K. A.; Francis, S. H.; Corbin, J. D. The structure of a bovine lung cGMP-binding, cGMP-specific phosphodiesterase deduced from a cDNA clone. *J. Biol. Chem.* **1993**, *268*, 22863–22873.
- (30) He, F.; Seryshev, A. B.; Cowan, C. W.; Wensel, T. G. Multiple zinc binding sites in retinal rod cGMP phosphodiesterase, PDE6 $\alpha\beta$. *J. Biol. Chem.* **2000**, *275*, 20572–20577.
- (31) Goldstein, I.; Lue, T. F.; Padma-Nathan, H.; Rosen, R. C.; Steers, W. D.; Wicker, P. A. Oral sildenafil in the treatment of erectile dysfunction. *N. Engl. J. Med.* **1998**, *338*, 1397–1404.
- (32) Daugan, A.; Grondin, P.; Ruault, C.; Le Monnier de Gouville, A.-C.; Coste, H.; Linget, J. M.; Kirilovsky, J.; Hyafil, F.; Labaudinière, R. The discovery of tadalafil: A novel and highly selective PDE5 inhibitor. 2: 2,3,6,7,12,12a-Hexahydropyrazino[1',2':1,6]pyrido[3,4-b]indole-1,4-dione analogues. *J. Med. Chem.* **2003**, *46*, 4533–4542. Peter, S.; Niels, S.; Hanna, T.; Helmut, H.; Erwin, B. Phosphodiesterase 5 inhibitors and erectile dysfunction. *Expert Opin. Ther. Pat.* **2008**, *18*, 21–33.
- (33) Sung, B.-J.; Hwang, K. Y.; Jeon, Y. H.; Lee, J. I.; Heo, Y.-S.; Kim, J. H.; Moon, J.; Yoon, J. M.; Hyun, Y.-L.; Kim, E.; Eum, S. J.; Park, S.-Y.; Lee, J.-O.; Lee, T. G.; Ro, S.; Cho, J. M. Structure of the catalytic domain of human phosphodiesterase 5 with bound drug molecules. *Nature* **2003**, *425*, 98–102.
- (34) Card, G. L.; England, B. P.; Suzuki, Y.; Fong, D.; Powell, B.; Lee, B.; Luu, C.; Tabrizizad, M.; Gillette, S.; Ibrahim, P. N.; Artis, D. R.; Bollag, G.; Milburn, M. V.; Kim, S.-H.; Schlessinger, J.; Zhang, K. Y. J. Structural basis for the activity of drugs that inhibit phosphodiesterases. *Structure* **2004**, *12*, 2233–2247.

- (35) Zhang, K. Y. J.; Card, G. L.; Suzuki, Y.; Artis, D. R.; Fong, D.; Gillette, S.; Hsieh, D.; Neiman, J.; West, B. L.; Zhang, C.; Milburn, M. V.; Kim, S.-H.; Schlessinger, J.; Bollag, G. A glutamine switch mechanism for nucleotide selectivity by phosphodiesterases. *Mol. Cell* **2004**, *15*, 279–286.
- (36) Wang, H.; Liu, Y.; Huai, Q.; Cai, J.; Zoragh, R.; Francis, S. H.; Corbin, J. D.; Robinson, H.; Xin, Z.; Lin, G.; Ke, H. Multiple conformations of phosphodiesterase-5: Implications for enzyme function and drug development. *J. Biol. Chem.* **2006**, *281*, 21469–21479.
- (37) Wang, H.; Ye, M.; Robinson, H.; Francis, S. H.; Ke, H. Conformational variations of both phosphodiesterase-5 and inhibitors provide the structural basis for the physiological effects of vardenafil and sildenafil. *Mol. Pharmacol.* **2008**, *73*, 104–110.
- (38) Piriev, N. I.; Yamashita, C.; Samuel, G.; Farber, D. B. Rod photoreceptor cGMP-phosphodiesterase: Analysis of α and β subunits expressed in human kidney cells. *Proc. Natl. Acad. Sci. U.S.A.* **1993**, *90*, 9340–9344.
- (39) Qin, N.; Baehr, W. Expression and mutagenesis of mouse rod photoreceptor cGMP phosphodiesterase. *J. Biol. Chem.* **1994**, *269*, 3265–3271.
- (40) Muradov, H.; Boyd, K. K.; Artemyev, N. O. Analysis of PDE6 function using chimeric PDE5/6 catalytic domains. *Vision Res.* **2006**, *46*, 860–868.
- (41) Palmer, M. J.; Bell, A. S.; Fox, D. N. A.; Brown, D. G. Design of second generation phosphodiesterase 5 inhibitors. *Curr. Top. Med. Chem.* **2007**, *7*, 405–419.
- (42) Kaczanowski, S.; Zielenkiewicz, P. Why do similar protein sequences encode similar three-dimensional structures? *Theor. Chem. Acc.* **2010**, *125*, 643–650.
- (43) Martí-Renom, M. A.; Stuart, A. C.; Fiser, A.; Sánchez, R.; Melo, F.; Šali, A. Comparative protein structure modeling of genes and genomes. *Annu. Rev. Biophys. Biomol. Struct.* **2000**, *29*, 291–325.
- (44) Accelrys Discovery Studio, version 2.5.5; Accelrys Software Inc.: San Diego, CA, 2010.
- (45) Case, D. A.; Darden, T. A.; Cheatham, T. E., III; Simmerling, C. L.; Wang, J.; Duke, R. E.; Luo, R.; Walker, R. C.; Zhang, W.; Merz, K. M.; Roberts, B. P.; Hayik, S.; Roitberg, A.; Seabra, G.; Swails, J.; Götz, A. W.; Kolossváry, I.; Wong, K. F.; Paesani, F.; Vanicek, J.; Wolf, R. M.; Liu, J.; Wu, X.; Brozell, S. R.; Steinbrecher, T.; Gohlke, H.; Cai, Q.; Ye, X.; Wang, J.; Hsieh, M. J.; Cui, G.; Roe, D. R.; Mathews, D. H.; Seetin, M. G.; Salomon-Ferrer, R.; Sagui, C.; Babin, V.; Luchko, T.; Gusarov, S.; Kovalenko, A.; Kollman, P. A. AMBER 11; University of California: San Francisco, 2010.
- (46) Wu, G.; Robertson, D. H.; Brooks, C. L.; Vieth, M. Detailed analysis of grid-based molecular docking: A case study of CDOCKER—A CHARMM-based MD docking algorithm. *J. Comput. Chem.* **2003**, *24*, 1549–1562.
- (47) Li, Z.; Cai, Y.-H.; Cheng, Y.-K.; Lu, X.; Shao, Y.-X.; Li, X.; Liu, M.; Liu, P.; Luo, H.-B. Identification of novel phosphodiesterase-4D inhibitors prescreened by molecular dynamics-augmented modeling and validated by bioassay. *J. Chem. Inf. Model.* **2013**, *53*, 972–981.
- (48) Chen, S.-K.; Zhao, P.; Shao, Y.-X.; Li, Z.; Zhang, C.; Liu, P.; He, X.; Luo, H.-B.; Hu, X. Moracin M from *Morus alba* L. is a natural phosphodiesterase-4 inhibitor. *Bioorg. Med. Chem. Lett.* **2012**, *22*, 3261–3264.
- (49) Stote, R. H.; Karplus, M. Zinc binding in proteins and solution: A simple but accurate nonbonded representation. *Proteins: Struct., Funct., Bioinf.* **1995**, *23*, 12–31.
- (50) Xiong, Y.; Lu, H.-T.; Li, Y.; Yang, G.-F.; Zhan, C.-G. Characterization of a catalytic ligand bridging metal ions in phosphodiesterases 4 and 5 by molecular dynamics simulations and hybrid quantum mechanical/molecular mechanical calculations. *Biophys. J.* **2006**, *91*, 1858–1867.
- (51) Massova, I.; Kollman, P. Combined molecular mechanical and continuum solvent approach (MM-PBSA/GBSA) to predict ligand binding. *Perspect. Drug Discovery Des.* **2000**, *18*, 113–135.
- (52) Liu, M.; Yuan, M.; Luo, M.; Bu, X.; Luo, H.-B.; Hu, X. Binding of curcumin with glyoxalase I: Molecular docking, molecular dynamics simulations, and kinetics analysis. *Biophys. Chem.* **2010**, *147*, 28–34.
- (53) He, L.; He, F.; Bi, H.; Li, J.; Zeng, S.; Luo, H.-B.; Huang, M. Isoform-selective inhibition of chrysanthemum towards human cytochrome P450 1A2. Kinetics analysis, molecular docking, and molecular dynamics simulations. *Bioorg. Med. Chem. Lett.* **2010**, *20*, 6008–6012.
- (54) Zhao, P.; Chen, S.-K.; Cai, Y.-H.; Lu, X.; Li, Z.; Cheng, Y.-K.; Zhang, C.; Hu, X.; He, X.; Luo, H.-B. The molecular basis for the inhibition of phosphodiesterase-4D by three natural resveratrol analogs. Isolation, molecular docking, molecular dynamics simulations, binding free energy, and bioassay. *Biochim. Biophys. Acta* **2013**, *1834*, 2089–2096.
- (55) Wang, J.; Hou, T.; Xu, X. Recent advances in free energy calculations with a combination of molecular mechanics and continuum models. *Curr. Comput.-Aided Drug Des.* **2006**, *2*, 287–306.
- (56) Hou, T.; Wang, J.; Li, Y.; Wang, W. Assessing the performance of the MM/PBSA and MM/GBSA methods. I. The accuracy of binding free energy calculations based on molecular dynamics simulations. *J. Chem. Inf. Model.* **2011**, *51*, 69–82.
- (57) Hou, T.; Wang, J.; Li, Y.; Wang, W. Assessing the performance of the molecular mechanics/Poisson Boltzmann surface area and molecular mechanics/generalized Born surface area methods. II. The accuracy of ranking poses generated from docking. *J. Comput. Chem.* **2011**, *32*, 866–877.
- (58) Xu, L.; Sun, H.; Li, Y.; Wang, J.; Hou, T. Assessing the performance of MM/PBSA and MM/GBSA methods. 3. The impact of force fields and ligand charge models. *J. Phys. Chem. B* **2013**, *117*, 8408–8421.
- (59) Still, W. C.; Tempczyk, A.; Hawley, R. C.; Hendrickson, T. Semianalytical treatment of solvation for molecular mechanics and dynamics. *J. Am. Chem. Soc.* **1990**, *112*, 6127–6129.
- (60) Sanner, M. F.; Olson, A. J.; Spehner, J.-C. Reduced surface: An efficient way to compute molecular surfaces. *Biopolymers* **1996**, *38*, 305–320.
- (61) Prime, version 3.1; Schrödinger, LLC: New York, 2012.
- (62) Molecular Operating Environment (MOE), version 2010.10; Chemical Computing Group Inc.: Montreal, QC, 2010.
- (63) Labute, P. The generalized Born/volume integral implicit solvent model: Estimation of the free energy of hydration using London dispersion instead of atomic surface area. *J. Comput. Chem.* **2008**, *29*, 1693–1698.
- (64) Baker, B. Y.; Palczewski, K. Detergents stabilize the conformation of phosphodiesterase 6. *Biochemistry* **2011**, *50*, 9520–9531.